



HAL
open science

Anthropogenic Release and Distribution of Titanium Dioxide Particles in a River Downstream of a Nanomaterial Manufacturer Industrial Site

Danielle L Slomberg, Melanie Auffan, Nelly Guéniche, Bernard Angeletti, Andrea Campos, Daniel Borschneck, Olivier Aguerre-Chariol, Jérôme Rose

► **To cite this version:**

Danielle L Slomberg, Melanie Auffan, Nelly Guéniche, Bernard Angeletti, Andrea Campos, et al.. Anthropogenic Release and Distribution of Titanium Dioxide Particles in a River Downstream of a Nanomaterial Manufacturer Industrial Site. *Frontiers in Environmental Science*, 2020, 8, 10.3389/fenvs.2020.00076 . hal-03043049

HAL Id: hal-03043049

<https://amu.hal.science/hal-03043049v1>

Submitted on 7 Dec 2020

HAL is a multi-disciplinary open access archive for the deposit and dissemination of scientific research documents, whether they are published or not. The documents may come from teaching and research institutions in France or abroad, or from public or private research centers.

L'archive ouverte pluridisciplinaire **HAL**, est destinée au dépôt et à la diffusion de documents scientifiques de niveau recherche, publiés ou non, émanant des établissements d'enseignement et de recherche français ou étrangers, des laboratoires publics ou privés.



Distributed under a Creative Commons Attribution 4.0 International License



Anthropogenic Release and Distribution of Titanium Dioxide Particles in a River Downstream of a Nanomaterial Manufacturer Industrial Site

Danielle L. Slomberg¹, Mélanie Auffan^{1,2}, Nelly Guéniche¹, Bernard Angeletti¹, Andrea Campos³, Daniel Borschneck¹, Olivier Aguerre-Chariol⁴ and Jérôme Rose^{1,2*}

¹ CNRS, Aix-Marseille Univ., IRD, INRAE, Coll France, CEREGE, Aix-en-Provence, France, ² Civil and Environmental Engineering Department, Duke University, Durham, NC, United States, ³ Aix-Marseille Univ., CNRS, Centrale Marseille, FSCM (FR1739), Marseille, France, ⁴ INERIS, Verneuil-en-Halatte, France

OPEN ACCESS

Edited by:

Denise M. Mitrano,
Swiss Federal Institute of Aquatic
Science and Technology, Switzerland

Reviewed by:

Kevin Wilkinson,
Université de Montréal, Canada
Mohammed Baalousha,
University of South Carolina,
United States

*Correspondence:

Jérôme Rose
rose@cerege.fr

Specialty section:

This article was submitted to
Biogeochemical Dynamics,
a section of the journal
Frontiers in Environmental Science

Received: 31 March 2020

Accepted: 18 May 2020

Published: 16 June 2020

Citation:

Slomberg DL, Auffan M, Guéniche N, Angeletti B, Campos A, Borschneck D, Aguerre-Chariol O and Rose J (2020) Anthropogenic Release and Distribution of Titanium Dioxide Particles in a River Downstream of a Nanomaterial Manufacturer Industrial Site. *Front. Environ. Sci.* 8:76. doi: 10.3389/fenvs.2020.00076

Several industries manufacture and process large quantities of engineered nanomaterials, thus increasing the potential for their environmental release during waste management and disposal. Herein, we quantified the release and spatial distribution of titanium dioxide nanomaterials (TiO₂ NMs) emitted from an industrial waste stream that flows into a nearby river. Two sampling campaigns were carried out on the river in fall 2017 and spring 2018 at selected sites upstream and downstream of the Industrial Effluent and an urban wastewater treatment plant (WWTP). Significant Ti accumulation was detected in the sediments at the Industrial Effluent and WWTP sites for both fall and spring samples, with measured Ti concentrations of 75–193 mg Ti/kg reaching 21–55× that of the local background upstream. X-ray diffraction analysis confirmed the anatase and rutile mineralogy of the inputs. River surface waters were filtered on-site to distinguish between particulate (>0.20 μm), colloidal (0.02–0.20 μm), and dissolved and/or small nanoparticulate (NP) (<0.02 μm) TiO₂. Up to 133 and 260 μg Ti/L were measured in the unfiltered waters for the Industrial Effluent and WWTP fall samples, respectively, while the spring samples exhibited Ti concentrations similar to the background concentration. Combining chemical analysis and scanning electron microscopy revealed that some Ti particles recovered from the Industrial Effluent and WWTP were clusters of TiO₂ NMs (~50 nm). Furthermore, anthropogenic TiO₂ was distinguished apart from natural Ti-containing minerals by comparing the concentration ratios between Ti and other naturally occurring elements (e.g., V, Al, and Fe). This study confirmed the release of manufactured TiO₂ NMs from the Industrial Effluent and the WWTP into the river, finding that almost all of the TiO₂ NMs are released in the particulate fraction (>0.20 μm), and that the particles sediment rapidly near the emission source and accumulate in the sediment.

Keywords: manufactured TiO₂ nanomaterials, anthropogenic emission, river ecosystem, environmental exposure, aggregation, sediment accumulation

INTRODUCTION

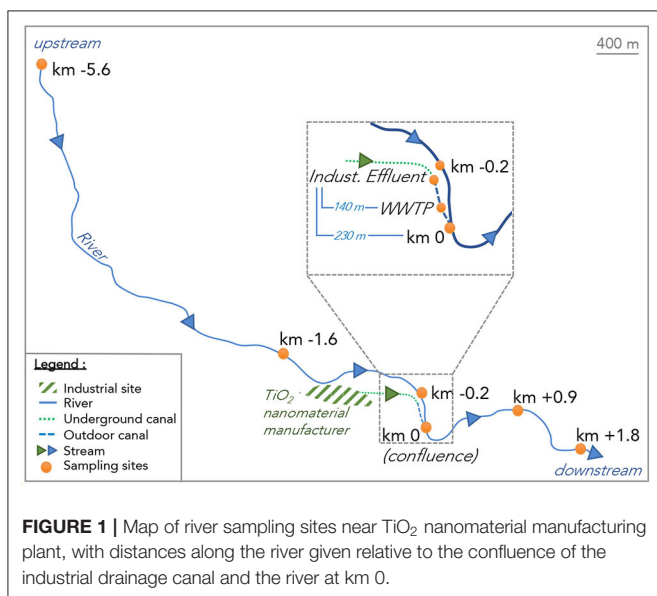
As advances in nanotechnology research and development continue, engineered nanomaterials are being increasingly manufactured for incorporation into consumer products destined for cosmetic, textile, coating, and plastic applications (Piccinno et al., 2012; Vance et al., 2015). Several recent studies have considered the environmental impacts of nanomaterials released from these consumer products during their use phase and end-of-life (Botta et al., 2011; Nowack et al., 2012; Mitrano et al., 2015; Auffan et al., 2018; Scifo et al., 2018), but another important consideration is the possible release and local environmental accumulation near nanomaterial manufacturing sites, especially those close to aquatic ecosystems such as rivers and lakes. Upon incidental or direct release into these natural systems, nanomaterial fate, and transport are governed by the water chemistry, particle aggregation state, and any transformation processes (e.g., dissolution, photochemical alteration, oxidation and reduction) (Nowack et al., 2012).

In the case of titanium dioxide nanomaterials (TiO₂ NMs), the second most-produced nanomaterial worldwide (Sun et al., 2014), previous research has already focused on evaluating their fate and behavior in model river waters, with the aim of determining their potential risk. Indeed, the aggregation and sedimentation of two of the most common TiO₂ NM forms, anatase and rutile, have been shown to depend on particle morphology, the point of zero charge, and water conditions (Liu et al., 2011; Iliina et al., 2017). Besides the physico-chemical characteristics of the TiO₂ NMs themselves and the pH of the aqueous environment, the presence of dissolved ions, suspended particulate matter (SPM), and natural organic matter (NOM) can also significantly influence NM stability through processes such as aggregation and sedimentation or dispersion and transport (Loosli et al., 2013; Labille et al., 2015; Slomberg et al., 2019). For example, increased ionic strength and divalent cation concentrations have been shown to facilitate TiO₂ NM homo-aggregate formation (Loosli et al., 2013; Iliina et al., 2017). However, in natural aqueous environments where SPM and NOM concentrations (mg/L) are likely much higher than the predicted TiO₂ NM concentration (μg/L), hetero-aggregation is expected to be the more dominant interaction driving NM fate and behavior (Labille et al., 2015). As such, Adam et al. evaluated both TiO₂ NM homo-aggregation and hetero-aggregation interactions with illite clay and Suwannee River fulvic acid (SRFA) in filtered river water (pH 8) sampled nearby the TiO₂ NM manufacturing site (Adam et al., 2016). In lower salinity conditions (0.25 mM Ca²⁺) the 5 nm TiO₂ particles (40 mg/L) formed homo-aggregates (~ 550 nm). The addition of SRFA (5–10 mg/L) slightly enhanced TiO₂ NM dispersion and decreased the overall TiO₂ aggregate size, and in the presence of illite (25 mg/L) no secondary hetero-aggregation was observed. Yet, when the river water Ca²⁺ concentration was increased to 3 mM, the decrease in TiO₂ NM homo-aggregate size was no longer observed in the presence of SRFA and the addition of illite resulted in hetero-aggregation, thus favoring NM sedimentation.

Multimedia environmental fate models have also been developed to investigate NM fate and transport in rivers as a

complement to experimental approaches. Any NM inputs into river surface waters should be detected almost instantaneously, although their lifetime in the water column may be transient due to aggregation processes and changes in hydrological conditions. For NMs that are not stable in the water column, the riverbed sediment can act as a sink where the NMs will deposit and potentially accumulate as long as the NM emission continues. For example, river box models incorporating fixed or varied water conditions in time and space have examined TiO₂ NM fate in surface waters and sediment for two large European rivers, the Rhine, and the Rhone (Praetorius et al., 2012; Sani-Kast et al., 2015). In both cases, for a constant, point source TiO₂ NM emission of 0.39–1.5 kg/day, predicted TiO₂ NM concentrations were in the ng/L range for the water compartment and mg/kg in the sediment. TiO₂ NM fate was dependent on the water conditions near the emission source, with significant aggregation, sedimentation, and accumulation in the sediment layer occurring within a few km of NM release. However, these models also predicted that a fraction of TiO₂ NMs can remain stable in the water column, being transported up to ~100 km from the source depending on river conditions.

While laboratory studies with simulated aquatic systems and the development of environmental fate models have allowed researchers to gain insight into TiO₂ NM transport, behavior, and fate, field studies to determine NM release and accumulation in real aqueous environments are still lacking. This is in part due to the fact that detecting and quantifying low concentrations of anthropogenic TiO₂ NMs apart from the natural background is analytically challenging. Recent approaches include a combination of size fractionation (e.g., filtration, field-flow fractionation) followed by identification and quantification using elemental analysis (i.e., inductively coupled plasma–mass spectrometry, ICP-MS) and electron microscopy coupled with X-ray energy dispersive spectroscopy (EDS) detection (Von der Kammer et al., 2011, 2012; Westerhoff et al., 2011; Labille et al., 2019). For example, three different sampling campaigns that analyzed filtered waters (<0.45 μm) near a wastewater treatment plant (WWTP) confirmed TiO₂ NM presence with electron microscopy and reported Ti values between 0.7 and 3 μg/L (Johnson et al., 2011; de Klein et al., 2016; Markus et al., 2018). Single particle (SP)-ICP-MS was utilized to target and detect smaller TiO₂ particles down to 100 nm in river surface waters without the need for filtration (Peters et al., 2018), and Hadioui et al. (2019) have now detected TiO₂ particle sizes down to 19.2 nm with the technique. While progress has been made in detecting low concentrations of TiO₂ NMs (μg/L) in complex environmental matrices, these analyses alone cannot confirm that the particles are anthropogenic. As such, the determination of elemental ratios between Ti and other naturally occurring elements such as V, Al, and Fe, or rare earth elements (Ga, Y, Nb, Eu, Ho, Er, Tm, Yb, Ta) has been employed to distinguish natural Ti-containing particles from the anthropogenic load in aquatic systems as well as soils (Gondikas et al., 2017; Reed et al., 2017; Labille et al., 2019; Baalousha et al., 2020; Wang et al., 2020). Building upon this approach, multi-element (ME)-SP-ICP-MS has been used to perform multi-element analysis of individual TiO₂ particles in



natural surface waters (Gondikas et al., 2018; Loosli et al., 2019). By identifying multi-element signatures of natural Ti-containing particles, anthropogenic TiO₂ NMs can be further distinguished apart from the natural background and quantified. Overall, these studies have demonstrated that TiO₂ NMs can be quantified in natural surface waters, while also providing insight as to their release from WWTPs or other anthropogenic sources. This knowledge is crucial for evaluating TiO₂ NM risk to aquatic ecosystems, yet a comprehensive assessment can only be obtained by also considering TiO₂ NM transport and accumulation in the sediment compartment in future field studies.

The present work reports the first quantification of TiO₂ NMs in a river next to a nanomaterial manufacturing plant, both upstream and downstream of the potential emission source (i.e., industrial drainage canal). Surface waters, sediments, and epilithic organisms were collected along the river and industrial drainage canal at two different time periods (October 2017 and March 2018) to assess any short-term, pulse occurrence vs. long-term accumulation in the different environmental compartments. In addition to TiO₂ quantification, anatase and rutile inputs into the river were distinguished from the local background using mineralogical analysis. Several elements (X = V, Al, and Fe) naturally co-occurring with Ti in suspended mineral particles were also quantified to determine Ti/X elemental ratios. Higher elemental ratios compared to the natural background were used as an indication of Ti of anthropogenic origin. By sampling the water and sediment compartments at multiple sites along the river, TiO₂ NM transport and fate were determined in a real release scenario.

MATERIALS AND METHODS

Sampling Campaigns

The samples were taken along a 7.4 km long transect in a watershed of about 160 km² at two different time periods, on

October 18th, 2017 and March 22nd, 2018. For these dates, outflows of $0.98 \pm 0.01 \text{ m}^3 \cdot \text{s}^{-1}$ and $4.89 \pm 0.01 \text{ m}^3 \cdot \text{s}^{-1}$ were respectively measured in the river at a hydrology station located ~7 km upstream from the confluence (<http://hydro.eaufrance.fr/>). The river is characterized by an average annual pH of 7.6–8.1, dissolved organic carbon (DOC) concentration of 1.8–2.3 mg/L, and total suspended sediment (TSS) concentration of ~5 mg/L (Hissler and Probst, 2006; Adam et al., 2016). Eight sampling stations were selected: 6 along the river, upstream and downstream of the TiO₂ nanomaterial manufacturing site, and 2 along the drainage canal where treated industrial and urban effluents join the river (Figure 1). The confluence between the drainage canal and the river was referred to as km 0. The 6 sampling stations along the river were located at 5.6 km (km -5.6), 1.6 km (km -1.6), and 0.2 km (km -0.2) upstream of the confluence (km 0) as well as 0.9 km (km +0.9) and 1.8 km (km +1.8) downstream of the confluence. The effluents from the TiO₂ NM manufacturing site first flow through an underground canal (not accessible) for a distance of ~1 km before the outdoor section of the drainage canal begins. The 2 sampling stations along this outdoor drainage canal were located at the beginning of the outdoor discharge of the manufacturing site's treated effluent (230 m upstream of the confluence, station called "Industrial Effluent") and at the outflow of the urban waste water treatment plant's (WWTP) treated effluent that also flows into the surface of the water column in the drainage canal (90 m upstream of the confluence, station called "WWTP"). No natural water sources are located along this drainage canal and it is surrounded by steep embankments. The distance between the drainage canal and the river at the Industrial Effluent sampling station is ~35 m. The water depth was ~20 cm in both the drainage canal and river in October 2017 and March 2018.

On-Site Water and Sediment Collection

Water samples were collected manually in the center of the riverbed. As soon as water samples are collected, the particle size distribution can change rapidly. It was therefore decided to filter on-site to avoid any modification of the size distribution. Water samples were filtered on-site using both 0.20 and 0.02 μm inorganic membrane syringe filters [Anodisc (Al₂O₃), Whatman, UK]. The raw, unfiltered waters and the 0.20 and 0.02 μm-filtered waters were then brought back to the laboratory and stored at 4°C for elemental analysis using inductively coupled plasma-mass spectrometry (ICP-MS). The membrane filters were dried 24 h at room temperature (protected from ambient dust particles) and stored at 4°C for scanning electron microscopy (SEM) observation. Water size fractionation was performed to quantify Ti in the particulate, colloidal, and dissolved fractions. The particulate and colloidal fractions were separated with 0.20 μm filters. Ideally, separation of the colloidal and dissolved fractions requires 1 or 3 K-Dalton membranes. The 0.02 μm inorganic membranes selected for the current work were therefore unable to isolate the "true" dissolved fraction, and instead resulted in a fraction composed of dissolved plus small nanoparticulate (NP) species. This choice was made due to the operational conditions needed for a fast separation on-site.

Surface sediment samples (down to ~2 cm depth) were brought up from the center of the canal/river using a 50 mL syringe. These sediments were sieved at 1 mm and then 250 μm to remove larger grains and the fraction <250 μm was freeze-dried and homogenized for X-ray diffraction (XRD) and ICP-MS analysis. Natural epilithic organisms were also collected to evaluate TiO₂ accumulation. Briefly, a few grams of epilithic organisms were scraped from sedimentary river rocks at 3 sites along the river (km -5.6, 0, +1.8) (**Figure S1**). To remove any loosely adhered, small particles, the epilithic organisms were first gently rinsed with ultrapure water on a 20 μm sieve, then freeze-dried and homogenized before analysis with ICP-MS.

Mineralogical Analysis

X-ray diffraction (XRD) was performed on sediment fractions (<250, 1–250, and <1 μm) from 4 sites (km -5.6, Industrial Effluent, WWTP, km +1.8) for samples from October 18, 2017 to evaluate the river's background mineralogy of Ti-based phases and any anthropogenic TiO₂ contributions. The sediment samples from March 2018 were not included in the XRD analysis since they exhibited a similar distribution of Ti concentrations compared to those from October 2017. Based on previous analysis on the river sediment, we hypothesized that the <250 μm sediment fraction may contain background minerals exhibiting strong signals (e.g., quartz and feldspars) that could make it difficult to distinguish potentially less intense signals of anatase or rutile TiO₂ (Hissler and Probst, 2006). Thus, an additional size separation was performed to remove the larger background minerals and obtain a finer sediment fraction of <1 μm .

Briefly, the <1 μm fraction was recovered according to Stokes law by re-suspending the <250 μm sediment in ultrapure water (5.56 g/L), sonicating 30 min to break up aggregates, allowing the sample to settle for 186 min, and then collecting the top 4 cm (quartz density = 2.65 g/cm³) (Rubey, 1933). The recovered <1 μm sediment, along with the remaining 1–250 μm fraction were freeze-dried and homogenized before XRD analysis.

The three sediment fractions (<250, 1–250, and <1 μm) were ground with a mortar and pestle before depositing them on XRD low-background silicon plates. The samples were then analyzed with a PANalytical X-Pert PRO (Limeil-Brevannes, France) diffractometer equipped with Co K α radiation (1.79 Å) at 40 kV and 40 mA. Each fraction was spun at 15 rpm and scanned with a 2 θ range of 4–75°, step size of 0.033° and time per step of 4.7 s. Quartz was used as an internal standard to correct displacement of peak positions.

Elemental Analysis

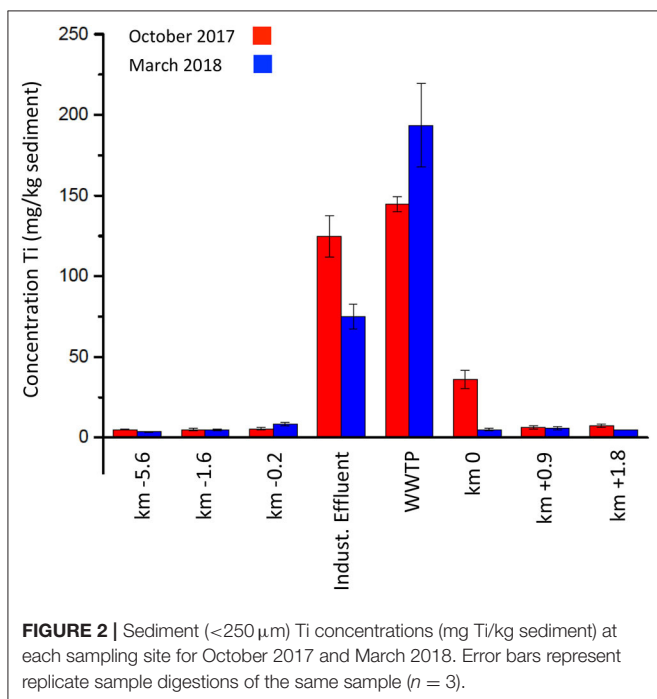
The fractioned sediment (<250 μm), surface waters, and epilithic organisms were subjected to total decomposition using microwave-assisted acid digestion before elemental analysis with ICP-MS. Fifty milligrams of the solid samples (i.e., sediments or epilithic organisms) were digested in an UltraWAVE microwave system (Milestone Inc.) with 1.5 mL HCl, 1 mL HNO₃, and 1 mL HF at 180°C. The raw and filtered surface water samples (2 mL) were digested in the same system with 1 mL HNO₃ and 0.5 mL HF. The digested residues were then diluted to

10 mL with ultrapure water before analysis for Ti, V, Al, and Fe concentrations using a PerkinElmer NexION 300X quadrupole ICP-MS (measured isotopes = ⁴⁷Ti, ⁵¹V, ²⁷Al, and ⁵⁶Fe). A 94–96% Ti recovery was measured for the above protocol using TiO₂ NP standards prepared in ultrapure water (0, 10, 50, 100, 500, and 1,000 $\mu\text{g/L}$). The concentrations of Na⁺, K⁺, Mg²⁺, and Ca²⁺ cations were determined by ICP-MS analysis (measured isotopes = ²³Na, ³⁹K, ²⁴Mg, and ⁴³Ca) of the 0.20 μm -filtered waters. The raw and filtered (0.20 and 0.02 μm) surface waters collected were analyzed for Ti concentration to provide insight into the real-time total, particulate (>0.20 μm), colloidal (0.02–0.20 μm), and dissolved and/or small nanoparticulate (<0.02 μm) Ti occurrence in the water column. The Ti concentrations in the particulate (>0.20 μm) fraction were calculated by subtracting the measured Ti in the 0.20 μm -filtered waters from the total Ti concentration in the raw surface waters. Likewise, the Ti concentration in the colloidal fraction (0.02–0.20 μm) was calculated by subtracting the Ti measured in the 0.02 μm -filtered waters from the Ti concentration measured in the 0.20 μm -filtered waters.

To distinguish natural and anthropogenic TiO₂ particles, we compared the elemental distributions of the collected natural samples (e.g., sediments and water) to two types of anthropogenic TiO₂ nanomaterials (NM1 and NM2) as well as 3 natural minerals (i.e., feldspar, clay, and quartz). NM1 and NM2 were provided as powders by the manufacturing plant located next to the sampled river. The anatase nanomaterials were well-crystallized and spherical, with a size of approximately 6.5 \pm 2.0 nm (NM1) and 38.8 \pm 2.0 nm (NM2) from transmission and scanning electron microscopy (**Figure S2**). It is also worth noting that the manufacturer not only produces nanomaterials, but also larger, submicron-sized pigments. The minerals analyzed were feldspar (albite and microcline of natural origin), clay (kaolinite), and quartz (<20 μm). The TiO₂ nanomaterials (i.e., NM1 and NM2) and minerals (50 mg) were digested using the same microwave-assisted procedure as that selected for the sediments and the resulting residues were diluted and analyzed with inductively coupled plasma-atomic emission spectroscopy (ICP-AES, Perkin Elmer 4300 DV) and ICP-MS for Ti, V, Al, and Fe concentrations.

Imagery and Elemental Detection

A Zeiss Gemini 500 scanning electron microscope (SEM) equipped with an EDAX Silicon Drift Detector was used to image and determine the elemental composition of surface water particles that had been collected on 0.20 μm inorganic membrane filters (Al₂O₃) on-site at the Industrial Effluent and WWTP discharge sites on October 18, 2017. One membrane filter from each site was attached directly to an aluminum pin stub with double-sided carbon tape and then analyzed without further preparation (e.g., sputter coating). In-lens secondary electron detection was employed for imaging and the microscope was operated at 1 kV with a working distance of 0.5 mm. Elemental analysis using Energy Dispersive Spectroscopy (EDS) was performed at 15 kV with a working distance of 12.3 mm to evaluate the presence of Ti, O, Al, Fe, and C.



RESULTS AND DISCUSSION

Ti Accumulation in Sediment Downstream of the Manufacturing Plant

The Ti concentrations in the river sediment were determined first to assess potential TiO₂ nanomaterial accumulation over time. As shown in **Figure 2**, similar trends in sediment Ti concentration were observed for the samples collected in October 2017 and March 2018 despite the seasonal differences of the two sampling campaigns. Upstream of the confluence, at km -5.6, -1.6, and -0.2, the background Ti concentration in the river sediment was stable at $\sim 5.4 \pm 1.5$ mg/kg. However, along the industrial drainage canal, the Ti concentrations in the sediment were ~ 21 – $25\times$ and ~ 29 – $55\times$ higher than the background for the Industrial Effluent and WWTP sites, respectively. Specifically, concentrations of 124.6 ± 12.6 and 75.1 ± 7.9 mg Ti/kg sediment were measured at the Industrial Effluent site, while 144.5 ± 4.6 and 193.6 ± 25.8 mg Ti/kg sediment were detected at the WWTP site for October 2017 and March 2018, respectively. While the measured Ti concentrations in the canal sediments were higher at the WWTP site compared to the Industrial Effluent discharge site, there is no indication that this increase is related to more Ti-containing particles being discharged from the WWTP effluent. Ti-containing particles discharged from the Industrial Effluent site may be transported ~ 90 m downstream before sedimenting at the WWTP site. Furthermore, although there appear to be significant differences in Ti sediment concentrations at the same site between October 2017 and March 2018, the presumed seasonal variations could also be due to difficulties in sampling the exact same sediment during both sampling campaigns. The two canal sites exhibited significant

Ti accumulation, yet downstream of the confluence (km 0), the sediment Ti concentrations returned to levels similar to those observed upstream. For example, in October 2017, some Ti accumulation (36.1 ± 5.7 mg/kg) was still observed at km 0, but the sediment Ti concentration at km +0.9 was 6.4 ± 1.0 mg/kg, which was similar to the upstream background of 4.9 ± 0.3 mg/kg at km -5.6. The sediments collected in March 2018 also exhibited little evidence of Ti accumulation downstream of the confluence and in fact, the Ti sediment concentration measured at km 0 was comparable to that at km -5.6 (4.9 ± 0.8 vs. 3.5 ± 0.4 mg Ti/kg sediment). However, elemental analysis alone cannot be used to verify that this increased Ti concentration in the sediment resulted from the presence of TiO₂ and not another Ti-containing mineral. Furthermore, complementary analyses are required to confirm that the detected Ti results from anthropogenic TiO₂.

Anthropogenic vs. Natural Origin of TiO₂ in Sediment

Anatase and rutile were not detected apart from the sediment background upstream at km -5.6 in the <1 and 1–250 μm sample fractions from October 2017 (**Figure 3A**). The presence of TiO₂ in the canal sediments at the Industrial Effluent and WWTP discharge sites was confirmed, with clear signals observed from both the anatase and rutile main peaks at 29.443 and 31.982 2θ [°], respectively (**Figure 3A**) (Swanson et al., 1969). Of note, the main quartz peak at 31.035 2θ [°] is also shown for reference. While anatase TiO₂ was detected in both the <1 and 1–250 μm sediment fractions at the Industrial Effluent site, this form was only detected in the <1 μm sediment fraction at the WWTP site. Similarly, rutile TiO₂ was detected in both sediment fractions at the Industrial Effluent site. No significant rutile presence was observed in the <1 μm sediment fraction at the WWTP site, however a strong signal was present in the 1–250 μm fraction. Downstream at km +1.8, the presence of anatase was observed in the <1 and 1–250 μm fractions, but rutile was not detectable (**Figure S3**). Although anatase and rutile TiO₂ both accumulated in the canal sediments at the Industrial Effluent and WWTP discharge sites, the two forms were concentrated differently within the two sediment size fractions, implying that the anatase and rutile TiO₂ detected at the two sites may not have the same primary particle size or be distributed within the sediment in the same way (e.g., aggregate formation). The two TiO₂ forms may also exhibit different stability and transport in the river water, as suggested by the fact that only the anatase form was detected downstream at km +1.8 (Fazio et al., 2008; Liu et al., 2011; Iswarya et al., 2015).

To go further in determining the origin of the anatase and rutile phases identified with XRD, Ti/X molar ratios (with X = V, Al, and Fe) of manufactured NMs (NM1 and NM2) and natural minerals (feldspar, clay, and quartz) were compared to the ratios found in the collected river sediments, as shown in **Figure 3B** (Gondikas et al., 2017, 2018; Reed et al., 2017). The total element concentrations used to calculate these ratios can be found in **Table S2**. Such analysis of other naturally occurring elements in the sediment was essential for determining whether

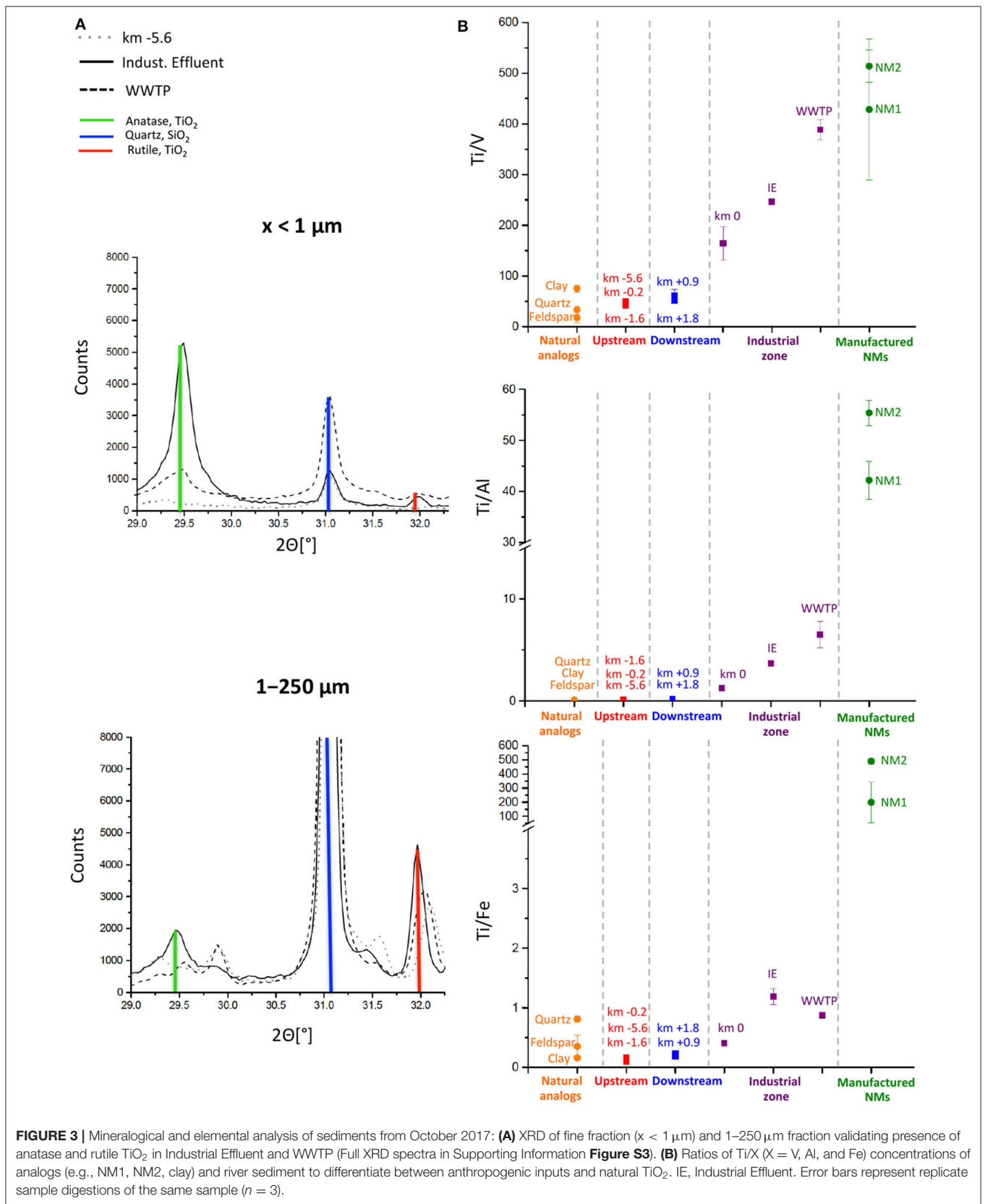


FIGURE 3 | Mineralogical and elemental analysis of sediments from October 2017: **(A)** XRD of fine fraction ($x < 1 \mu\text{m}$) and 1–250 μm fraction validating presence of anatase and rutile TiO₂ in Industrial Effluent and WWTP (Full XRD spectra in Supporting Information **Figure S3**). **(B)** Ratios of Ti/X (X = V, Al, and Fe) concentrations of analogs (e.g., NM1, NM2, clay) and river sediment to differentiate between anthropogenic inputs and natural TiO₂. IE, Industrial Effluent. Error bars represent replicate sample digestions of the same sample ($n = 3$).

these TiO₂ particles were anthropogenic or of natural origin. However, it must be considered that the comparison of Ti/X ratios using bulk elemental analysis measurements is based on the assumption that the natural background is best represented by individual, multi-element Ti-containing particles and not just the presence of numerous different particle compositions (e.g., Fe_xAl_yTi_zO_a vs. Fe_xO_y, TiO₂, and Al_xO_y). NM1 and NM2 exhibited Ti/V, Ti/Al, and Ti/Fe ratios of 428–513, 42–55, and 199–490, respectively, in marked contrast to the ratios of 18–75, 0.01–0.1, and 0.16–0.81 measured in natural feldspar, clay, and quartz analogs. The manufactured NMs contain minimal amounts of V, Al, and Fe compared to Ti, which significantly increases the Ti/X ratio. In contrast, the feldspar, clay, and quartz contain naturally present V, Al, and Fe, resulting in a lower Ti/X ratio. Considering the natural river samples, the canal sediments at the Industrial Effluent and WWTP discharge sites exhibited much higher Ti/X ratios compared to the other sites. Specifically, Ti/V, Ti/Al, and Ti/Fe ratios of 246–389, 3.7–6.5, and 0.87–1.19 were determined for the Industrial Effluent and WWTP sites whereas at km –5.6 these same ratios were 49, 0.12, and 0.15. The sediment at km 0 (confluence of the industrial drainage canal and the river) was also characterized by elevated Ti/X ratios compared to the other sites. Of the element ratios tested here, Ti/V was the strongest indicator of anthropogenic Ti origin, due to a lower and less variable natural background of V compared to Al and Fe, as well as the possibility of Al and Fe contamination from the industrial canal sites. In fact, the manufacturing plant uses ilmenite (FeTiO₃) for TiO₂ NM production and WWTPs are known to use Al- and Fe-based salts in their treatment processes (Liu et al., 2013). The elemental analysis results shown here are for the sediments collected in October 2017, but the same trends were revealed for the sediments collected in March 2018 (Figure S4).

While the Ti/X ratios for the sediments at the Industrial Effluent and WWTP discharge sites, and at km 0 were not as high as those of the pure TiO₂ NMs, their significantly elevated values combined with the mineralogy determined by XRD support the anthropogenic and non-natural origin of the TiO₂ in the surface sediment. In order to elucidate the potential sources (e.g., industrial drainage canal or river) of this long-term anthropogenic TiO₂ sediment accumulation, the Ti concentrations in the surface waters were measured for each site.

Real-Time TiO₂ Occurrence in the Surface Waters

The total Ti concentrations measured in the raw surface waters collected in October 2017 exhibited a similar trend to that observed in the sediments, with low Ti background levels (3.4–7.0 μg/L) at km –5.6, –1.6, and –0.2, and significant increases in Ti at both the Industrial Effluent and WWTP sites, up to 133 and 260 μg Ti/L, respectively (Figure 4). Again, due to particle transport, TiO₂ particles originating from the Industrial Effluent likely contributed to increased Ti concentrations at the WWTP site (Praetorius et al., 2012; Sani-Kast et al., 2015). Downstream of the drainage canal, Ti concentrations in the water column did not return to upstream background levels, even at km +1.8 after

the confluence, where the Ti concentration remained elevated (56.6 ± 8.6 μg/L). This finding is in support of river fate model predictions that have indicated that TiO₂ NMs can be transported several kilometers before settling into the sediment.

In March 2018, the Ti concentrations in the surface waters did not show any evolution along the industrial drainage canal or the river. At every sampling site, the Ti concentrations were comparable to that measured upstream at km –5.6 (4.9 ± 1.4 μg/L), even at the Industrial Effluent and WWTP discharge sites, where the measured concentrations were 3.4 ± 2.8 and 1.8 ± 0.5 μg/L, respectively. The disparate differences in total Ti detected in the surface waters between the two sampling dates could be the result of changes in waste management by the nanomaterial manufacturer (e.g., discharge), variations in canal flow, or due to seasonal dilution effects (e.g., rain or snowmelt) (Thompson, 1982; Carling et al., 2015). Indeed, changes in cation concentrations (Table S1) and the river outflow at km –5.6 between October 2017 and March 2018 suggest some dilution effects in the river. In October 2017 at km –5.6, the river outflow was 0.98 ± 0.01 m³.s⁻¹ and Na⁺ and Ca²⁺ concentrations were 0.497 and 0.207 mM, respectively, whereas in March 2018, the river outflow was ~ 5× higher at 4.89 ± 0.01 m³.s⁻¹ and the cation concentrations were lower (0.294 mM Na⁺ and 0.157 mM Ca²⁺). However, the low Ti concentrations detected in the surface waters at the Industrial Effluent and WWTP sites in March 2018 were more likely related to industrial waste management and differences in discharge since Na⁺ (0.308–6.26 mM) and Ca²⁺ (0.204–0.219 mM) concentrations in March 2018 were either similar or higher than in October 2017 (0.5–2.07 mM Na⁺ and 0.226–0.284 mM Ca²⁺) and water depth was comparable between the two seasons.

Similar to the analysis conducted for the sediments, Ti/X ratios (X = V, Al, Fe) were also calculated for the surface waters collected in October 2017 to discriminate between an anthropogenic vs. natural origin of the detected Ti (Figure 5). The Ti/X ratios were not calculated for the surface waters from March 2018 since no significant Ti was detected. The total element concentrations in the surface waters can be found in Table S3. At the Industrial Effluent, the determined Ti/V, Ti/Al, and Ti/Fe ratios were ~14× higher (ratios of 149, 1.13, and 1.27, respectively) than the ratios measured for the upstream sites (5–10, 0.05–0.08, and 0.08–0.09, respectively). Moving along the industrial drainage canal, Ti/X ratios in the WWTP surface water also remained elevated (4.5–15×) compared to those upstream. In contrast to the sediments where Ti/X ratios downstream of km 0 were similar to those upstream as a result of minimal anthropogenic Ti accumulation, in the surface waters Ti/V, Ti/Al, and Ti/Fe ratios remained elevated at km 0, +0.9, and +1.8 (31–51, 0.14–0.32, and 0.19–0.33). These complementary analyses of the surface water Ti/X ratios confirm the anthropogenic Ti emission from the Industrial Effluent and WWTP sites in October 2017. This demonstrates that the Ti measured in the surface waters downstream of the confluence resulted from the transport of anthropogenic material, not just the re-suspension of natural Ti in the sediment.

Using this data, the contribution of anthropogenic TiO₂ to the total Ti in the surface waters collected in October 2017 was

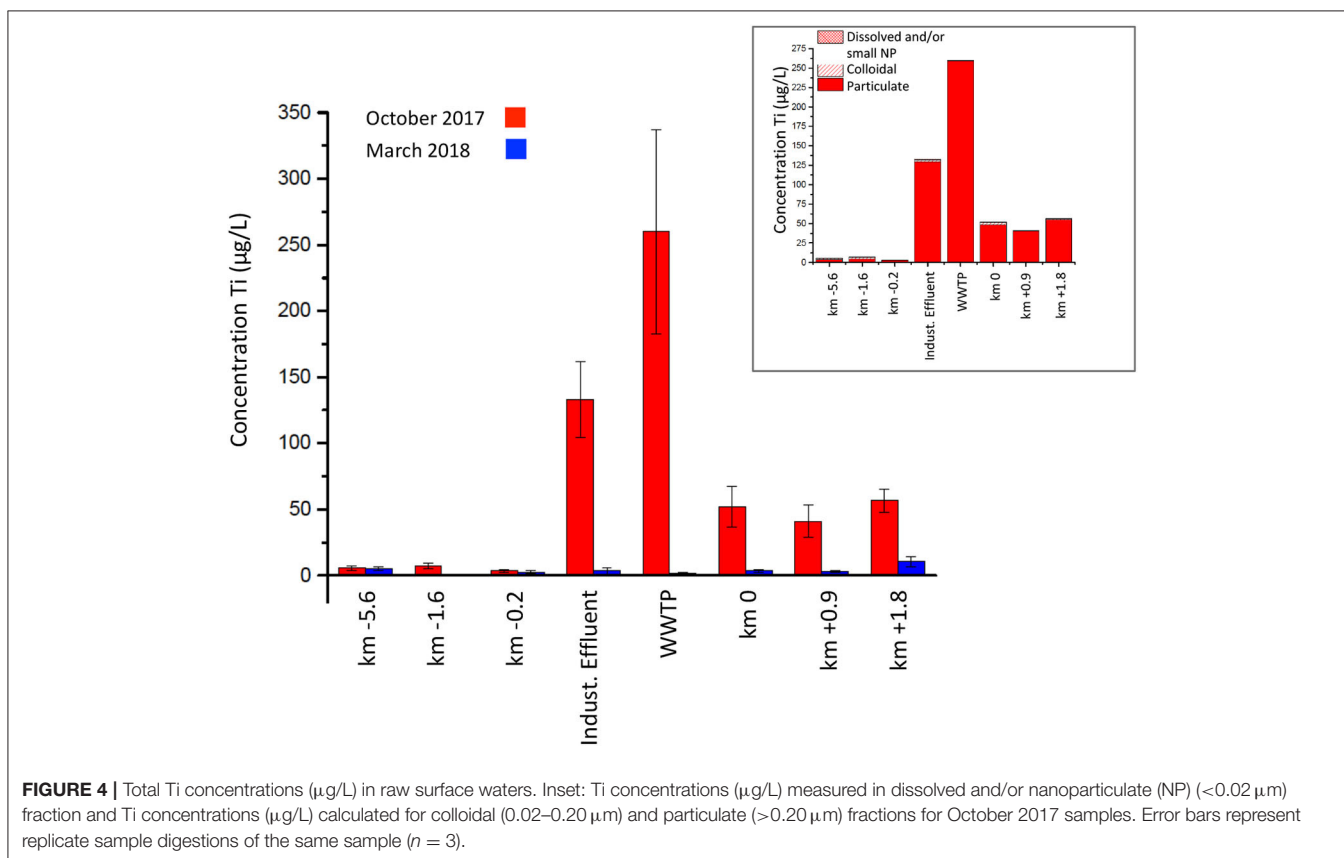


FIGURE 4 | Total Ti concentrations (µg/L) in raw surface waters. Inset: Ti concentrations (µg/L) measured in dissolved and/or nanoparticulate (NP) (<0.02 µm) fraction and Ti concentrations (µg/L) calculated for colloidal (0.02–0.20 µm) and particulate (>0.20 µm) fractions for October 2017 samples. Error bars represent replicate sample digestions of the same sample (n = 3).

estimated using Equation (1), as previously detailed in Loosli et al. (2019). These estimations are based on the assumption that all Ti measured above the background was in the form of pure TiO₂.

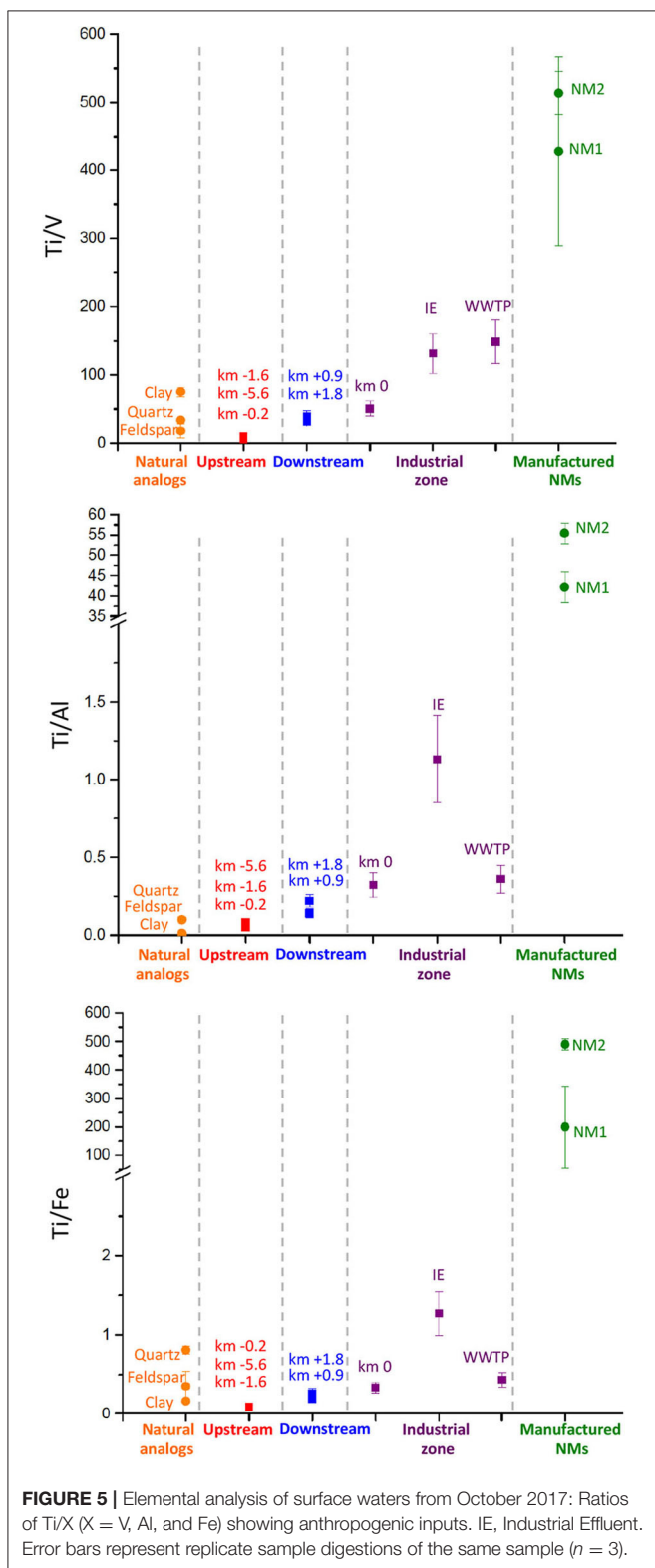
$$[\text{TiO}_2]_{\text{anthropogenic}} = \frac{\text{TiO}_{2\text{MM}}}{\text{Ti}_{\text{MM}}} \left[\text{Ti}_{\text{sample}} - V_{\text{sample}} \left(\frac{\text{Ti}}{V} \right)_{\text{background}} \right] \quad (1)$$

where [TiO₂]_{anthropogenic} is the estimated concentration of anthropogenic TiO₂, Ti_{MM} and TiO_{2MM} are the molar masses (MM) of Ti and TiO₂, Ti_{sample} and V_{sample} are the total mass concentrations, and Ti/V is the molar mass ratio of Ti to V. The background Ti/V ratio was calculated using the average Ti/V ratios measured at the three upstream sampling locations (i.e., km -5.6, -1.6, -0.2). For the Industrial Effluent and WWTP sites along the drainage canal, estimated TiO_{2anthropogenic} concentrations were 209 and 411 µg/L, representing 94 and 95% of the measured total Ti in the surface water, respectively. As expected, the estimated TiO_{2anthropogenic} concentrations downstream at the km 0 and km +1.8 sites were lower at 73 and 71 µg/L, representing 85 and 76% of the measured total Ti in the surface water, respectively.

Beyond validating the origin of the TiO₂ release, evaluating the size of the emitted particles is crucial for predicting their transport, fate, and potential toxicity. The October 2017 surface waters were filtered to look for the presence of TiO₂ in the particulate (>0.20 µm), colloidal (0.02–0.20 µm), and

dissolved and/or small nanoparticulate (<0.02 µm) fractions. Filtration and elemental analysis were also performed for the March 2018 samples, but due to low Ti concentrations in the raw surface waters, Ti in the filtrates was below 2 nM and not quantifiable (results not shown). As shown in the **Figure 4** inset, for the TiO₂ emitted from the Industrial Effluent and WWTP and then transported to the confluence at km 0, the majority of Ti was in the particulate form (98.6, 99.8, and 94% for the three sites, respectively), with a small contribution from the colloidal and dissolved and/or nanoparticulate fractions (0.2–6%). Specifically, Ti concentrations in the colloidal fraction were calculated to be 1.8, 0.4, and 3.1 µg/L for the Industrial Effluent, WWTP, and km 0 sites, whereas Ti concentrations measured in the dissolved/nanoparticulate fraction were 1.5, 0.3, and 0.4 µg/L for the respective sites. However, caution must be taken in interpreting these results, as previous work has shown that TiO₂ NMs can homo- and hetero- aggregate under river water conditions to form µm-sized aggregates (Loosli et al., 2013; Labille et al., 2015; Adam et al., 2016). Thus, the elemental analysis of the filtrates performed here cannot be used to distinguish between the presence of primary TiO₂ particles >0.20 µm and aggregates containing primary TiO₂ particles <0.20 µm.

Scanning electron microscopy (SEM) was used to visualize potential anthropogenic TiO₂ particles collected on 0.20 µm filter membranes from the Industrial Effluent and WWTP surface



waters in October 2017. Although such an analysis remains challenging due to the low amount of Ti and considerable difficulty in providing statistically relevant data, it provided information on the primary particle size and morphology.

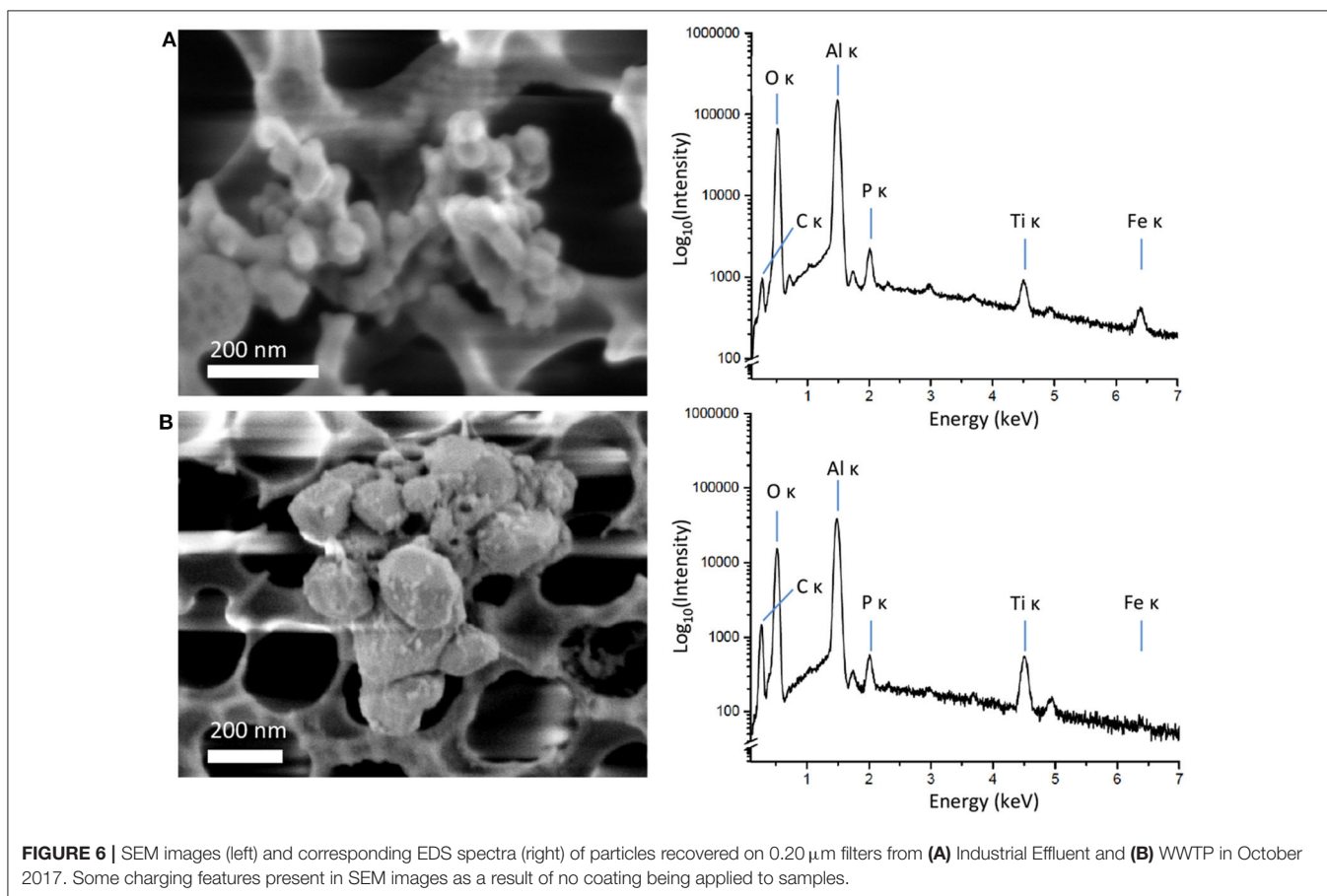
The resulting SEM images revealed the presence of clusters of spherical nanomaterials in the waters collected from the Industrial Effluent and WWTP, with a shape and size consistent of TiO₂ synthesized for industrial and commercial applications (Figure 6) (Westerhoff et al., 2011). For the Industrial Effluent (Figure 6A), the nanomaterials in the imaged cluster had a primary particle size of 50 ± 13 nm (1 image, $n = 11$ particles), whereas for the WWTP (Figure 6B), the primary particle size was larger at 174 ± 43 nm (1 image, $n = 8$ particles). Furthermore, both EDS spectra exhibited Ti K and O K peaks, confirming that the particles were TiO₂. Of note, the presence of some P and Fe can be attributed to the surrounding environment, while the large Al signal resulted from the aluminum oxide membrane filter and the SEM pin stub. Additional SEM images and EDS spectra of other regions on the same 0.20 μ m filter membranes also showed clusters of spherical TiO₂ nanomaterials, with primary particle sizes of ~ 50 – 150 nm (Figures S5–S7).

While Ti elemental analysis of the surface water fractions suggested that $>94\%$ of the emitted TiO₂ particles were >0.20 μ m, primary TiO₂ particles observed with SEM were <0.20 μ m, and should have passed through the 0.20 μ m membrane pores during filtration. These results indicate that the anthropogenic TiO₂ in the canal waters likely exists as aggregates of nanomaterials, at least in the Industrial Effluent. However, without further investigation it is not possible to discriminate between aggregates of fused TiO₂ nanomaterials formed during manufacturing from individual TiO₂ nanomaterials incorporated in homo- or hetero-aggregates formed in the canal waters under favorable ionic strength conditions (Loosli et al., 2013; Adam et al., 2016; Ilina et al., 2017; Slomberg et al., 2019). The formation of TiO₂ NM homo-aggregates over hetero-aggregates in the canal waters would only be probable if the NMs were present at a far greater concentration compared to that of natural colloids (Figure S8).

The significant differences in size of the TiO₂ particles collected at the Industrial Effluent and WWTP in October 2017 may result from temporal variations in particle manufacturing (production of nanomaterial and pigment), waste treatment, and effluent emissions. Furthermore, the disparity between the particles collected at the Industrial Effluent and the WWTP is coherent with the fact that the effluents from the NM manufacturing plant and the urban WWTP are unlikely to have the same composition. Any NMs present in the industrial effluent would be presumably composed of a mixture of unaged anatase and rutile TiO₂ based on plant production schedules, while those released in WWTP effluents most likely have a different origin and come from aged by-products of paints and personal care products (e.g., toothpaste, cosmetics) (Westerhoff et al., 2011).

Environmental Exposure Implications: TiO₂ Nanomaterial Release and Transport

The aggregation state of engineered nanomaterials in aqueous environments is a crucial parameter for predicting their residence time in the water column, their potential accumulation in the



sediment layer, and determining which organisms are at risk of exposure. In addition to the TiO₂ NM clusters observed with SEM (**Figure 6**), the distributions of the measured Ti concentrations in the sediments and surface water fractions along the industrial drainage canal and river are also in support of the presence of TiO₂ NM aggregates that sediment close to the emission source. As evidenced in **Figure 2**, the TiO₂ NMs accumulate in the canal sediment close to the sources of the Industrial Effluent and WWTP discharge. Downstream of the confluence, the measured NM accumulation was not significant, with the TiO₂ detected at km +1.8 representing only ~2% of that detected in the canal sediments near the two sources. However, due to the non-negligible TiO₂ background in the sediments (~5 mg/kg), minor changes in accumulation can be difficult to verify with elemental analysis. The presence and accumulation of anatase TiO₂ in sediments at km +1.8 were thus confirmed by complementary XRD analysis (**Figure S3**), further supporting that there is some TiO₂ NM transport downstream even though the majority of TiO₂ sedimentation occurs near the emission source. We also evaluated the potential of epilithic organisms to accumulate Ti by scraping them from sedimentary river rocks and analyzing them for Ti concentration. These epilithic organisms (and possible associated sediment remaining after rinsing) from both October 2017 and March 2018 showed signs of significant Ti

accumulation near the source, with concentrations of 3.3–5.8, 15.4–53.6, and 9.8–11.8 mg Ti/kg (dry weight) at km –5.6, 0, and +1.8. The Ti/V molar ratios of 53–68, 144–224, and 38–61 in the epilithic organisms at km –5.6, 0, and +1.8 also support an accumulation of anthropogenic Ti at km 0. As primary producers, these epilithic organisms represent the bottom of the trophic chain in the river ecosystem. Their TiO₂ accumulation thus provides a potential exposure pathway for primary consumers that feed on the sediments and subsequent entry into the food web.

Here, the canal and river sediments were a strong indicator of long-term NM accumulation, with similar TiO₂ concentrations observed for October 2017 and March 2018 along the various sites, including the Industrial Effluent, WWTP, and km 0. Yet, the sediment TiO₂ concentrations were not sensitive enough to provide information on real-time occurrence due to the difficulty in distinguishing small changes from a high background. The surface waters, having a low Ti background (3.4–7.0 μg Ti/L), offered a better indication of NM pulse release and transport mechanisms. As previously detailed, Ti concentrations in surface waters in October 2017 and March 2018 varied significantly (**Figure 4**), suggesting that NM emission in the canal was not constant and that environmental conditions (e.g., canal and river flow, seasonal dilution) may also play a role in NM detection. In October 2017, more significant transport was observed in the

surface water compared to what was revealed by the sediments. Downstream of the confluence at km +1.8, 20–40% of the TiO₂ detected at the emission sources remained in suspension. Thus, the processes of NM aggregation, sedimentation, and transport would likely continue further downstream of km +1.8. Indeed, TiO₂ NM fate model predictions have found that significant downstream transport is possible (Praetorius et al., 2012; Sani-Kast et al., 2015).

CONCLUSIONS

The thorough characterization of the surface water and sediment in a river next to a TiO₂ NM manufacturing plant highlighted both the presence and transport of anthropogenic TiO₂ NMs in the river ecosystem. Overall, the anthropogenic NMs exhibited rapid sedimentation near the TiO₂ emission source, but transport was still detected ~2 km downstream. It was also evidenced that the anthropogenic Ti transport occurred mainly via the particulate fraction (>0.20 μm) as aggregates in the water column. Emissions into the surface waters were likely transient due to industrial/WWTP management, but differences in measured Ti concentrations could also result from contrasting seasonal conditions in October 2017 and March 2018. Despite differences in real-time surface water concentrations, long-term anthropogenic TiO₂ accumulation was observed in the sediments near the source of the treated industrial effluents, but further work is needed to confirm the presence and distribution of TiO₂ NMs in these sediments. Future studies should also include additional sampling sites near the emission sources and downstream to provide a more detailed and spatially resolved understanding of the TiO₂ NM transport and sedimentation. Sampling over several time periods will also be crucial for evaluating the transient nature of the TiO₂ NMs detected in the surface waters. The influence of these NMs on river organisms should also be further evaluated, investigating the effects of the TiO₂ NMs on several organisms in the trophic chain (primary producers and consumers) using relevant concentrations and considering pulse vs. chronic exposures.

REFERENCES

- Adam, V., Loyaux-Lawnczak, S., Labille, J., Galindo, C., del Nero, M., Gangloff, S., et al. (2016). Aggregation behaviour of TiO₂ nanoparticles in natural river water. *J. Nanopart. Res.* 18:13. doi: 10.1007/s11051-015-3319-4
- Auffan, M., Liu, W., Brousset, L., Scifo, L., Pariat, A., Sanles, M., et al. (2018). Environmental exposure of a simulated pond ecosystem to a CuO nanoparticle-based wood stain throughout its life cycle. *Environ. Sci. Nano* 5, 2579–2589. doi: 10.1039/C8EN00712H
- Baalousha, M., Wang, J., Nabi, M. M., Loosli, F., Valenca, R., Mohanty, S. K., et al. (2020). Stormwater green infrastructures retain high concentrations of TiO₂ engineered (nano)-particles. *J. Hazard Mater.* 392:122335. doi: 10.1016/j.jhazmat.2020.122335
- Botta, C., Labille, J., Auffan, M., Borschneck, D., Miche, H., Cabié, M., et al. (2011). TiO₂-based nanoparticles released in water from commercialized sunscreens in a life-cycle perspective: structures and quantities. *Environ. Pollut.* 159, 1543–1550. doi: 10.1016/j.envpol.2011.03.003
- Carling, G. T., Tingey, D. G., Fernandez, D. P., Nelson, S. T., Aanderud, Z. T., Goodsell, T. H., et al. (2015). Evaluating natural and anthropogenic trace element inputs along an alpine to urban gradient in the Provo River, Utah, USA. *Appl. Geochem.* 63, 398–412. doi: 10.1016/j.apgeochem.2015.10.005
- de Klein, J. J., Quik, J. T., Bäuerlein, P. S., and Koelmans, A. A. (2016). Towards validation of the NanoDUFLOW nanoparticle fate model for the river Dommel, The Netherlands. *Environ. Sci. Nano* 3, 434–441. doi: 10.1039/C5EN00270B
- Fazio, S., Guzman, J., Colomer, M., Salomoni, A., and Moreno, R. (2008). Colloidal stability of nanosized titania aqueous suspensions. *J. Eur. Ceram. Soc.* 28, 2171–2176. doi: 10.1016/j.jeurceramsoc.2008.02.017
- Gondikas, A., von der Kammer, F., Kaegi, R., Borovinskaya, O., Neubauer, E., Navratilova, J., et al. (2018). Where is the nano? Analytical approaches for the detection and quantification of TiO₂ engineered nanoparticles in surface waters. *Environ. Sci. Nano* 5, 313–326. doi: 10.1039/C7EN00952F
- Gondikas, A. P., Kammer, F., Reed, R. B., Wagner, S., Ranville, J. F., and Hofmann, T. (2017). Release of TiO₂ nanoparticles from sunscreens into surface waters: a one-year survey at the old Danube recreational Lake. *Environ. Sci. Technol.* 48, 5415–5422. doi: 10.1021/es405596y
- Hadioui, M., Knapp, G., Azimzada, A., Jreije, I., Frechette-Viens, L., and Wilkinson, K. J. (2019). Lowering the size detection limits of Ag and TiO₂

DATA AVAILABILITY STATEMENT

The raw data supporting the conclusions of this article will be made available by the authors, without undue reservation.

AUTHOR CONTRIBUTIONS

MA and JR collected samples along the river and industrial drainage canal. DS prepared and conducted elemental analysis of the water, sediment, and epilithic organism samples with the help of NG and BA. DS and DB prepared and analyzed sediment samples with XRD. DS, MA, AC, and JR prepared and analyzed filter membranes with SEM. DS, MA, AC, DB, OA-C, and JR contributed to the interpretation of data. DS, MA, AC, OA-C, and JR contributed to the writing of the manuscript. All authors contributed to the article and approved the submitted version.

ACKNOWLEDGMENTS

This work was financed in part by the French Agency for the Environmental and Energetic Management (ADEME) under the contract number 1581C0027 called NANO-IDENT, funded by the 2015 CORTEA call. This work is a contribution to the OSU-Institut Pythéas, and to the Labex Serenade program (no. ANR-11-LABX-0064) funded by the Investissements d'Avenir program of the French National Research Agency (ANR) through the A*MIDEX project (no. ANR-11-IDEX-0001-02). The authors acknowledge the CNRS for the funding of the IRP iNOVE.

SUPPLEMENTARY MATERIAL

The Supplementary Material for this article can be found online at: <https://www.frontiersin.org/articles/10.3389/fenvs.2020.00076/full#supplementary-material>

- nanoparticles by single particle ICP-MS. *Anal. Chem.* 91, 13275–13284. doi: 10.1021/acs.analchem.9b04007
- Hissler, C., and Probst, J.-L. (2006). Chlor-alkali industrial contamination and riverine transport of mercury: distribution and partitioning of mercury between water, suspended matter, and bottom sediment of the Thur River, France. *Appl. Geochem.* 21, 1837–1854. doi: 10.1016/j.apgeochem.2006.08.002
- Iliina, S. M., Ollivier, P., Slomberg, D., Baran, N., Pariat, A., Devau, N., et al. (2017). Investigations into titanium dioxide nanoparticle and pesticide interactions in aqueous environments. *Environ. Sci. Nano* 4, 2055–2065. doi: 10.1039/C7EN00445A
- Iswarya, V., Bhuvaneshwari, M., Alex, S. A., Iyer, S., Chaudhuri, G., Chandrasekaran, P. T., et al. (2015). Combined toxicity of two crystalline phases (anatase and rutile) of Titania nanoparticles towards freshwater microalgae: *Chlorella* sp. *Aquat. Toxicol.* 161, 154–169. doi: 10.1016/j.aquatox.2015.02.006
- Johnson, A. C., Bowes, M. J., Crossley, A., Jarvie, H. P., Jurkschat, K., Jürgens, M. D., et al. (2011). An assessment of the fate, behaviour and environmental risk associated with sunscreen TiO₂ nanoparticles in UK field scenarios. *Sci. Tot. Environ.* 409, 2503–2510. doi: 10.1016/j.scitotenv.2011.03.040
- Labille, J., Harns, C., Bottero, J.-Y., and Brant, J. (2015). Heteroaggregation of titanium dioxide nanoparticles with natural clay colloids under environmentally relevant conditions. *Environ. Sci. Technol.* 48, 10690–10698. doi: 10.1021/es501655v
- Labille, J., Slomberg, D., Catalano, R., Robert, S., Apers-Tremelo, M.-L., Boudenne, J.-L., et al. (2019). Assessing UV filter inputs into beach waters during recreational activity: a field study of three French Mediterranean beaches from consumer survey to water analysis. *Sci. Tot. Environ.* 2019:136010. doi: 10.1016/j.scitotenv.2019.136010
- Liu, X., Chen, G., and Su, C. (2011). Effects of material properties on sedimentation and aggregation of titanium dioxide nanoparticles of anatase and rutile in the aqueous phase. *J. Coll. Int. Sci.* 363, 84–91. doi: 10.1016/j.jcis.2011.06.085
- Liu, Y., Zhang, W., Yang, X., Xiao, P., Wang, D., and Song, Y. (2013). Advanced treatment of effluent from municipal WWTP with different metal salt coagulants: contaminants treatability and floc properties. *Sep. Purif. Technol.* 120, 123–128. doi: 10.1016/j.seppur.2013.09.046
- Loosli, F., Le Coustumer, P., and Stoll, S. (2013). TiO₂ nanoparticles aggregation and disaggregation in presence of alginate and Suwannee River humic acids: pH and concentration effects on nanoparticle stability. *Water Res.* 47, 6052–6063. doi: 10.1016/j.watres.2013.07.021
- Loosli, F., Wang, J., Rothenberg, S., Bizimis, M., Winkler, C., Borovinskaya, O., et al. (2019). Sewage spills are a major source of titanium dioxide engineered (nano)-particle release into the environment. *Environ. Sci. Nano* 6, 763–777. doi: 10.1039/C8EN01376D
- Markus, A., Krystek, P., Tromp, P., Parsons, J., Roex, E., de Voogt, P., et al. (2018). Determination of metal-based nanoparticles in the river Dommel in the Netherlands via ultrafiltration, HR-ICP-MS and SEM. *Sci. Tot. Environ.* 631, 485–495. doi: 10.1016/j.scitotenv.2018.03.007
- Mitrano, D. M., Motellier, S., Clavaguera, S., and Nowack, B. (2015). Review of nanomaterial aging and transformations through the life cycle of nano-enhanced products. *Environ. Int.* 77, 132–147. doi: 10.1016/j.envint.2015.01.013
- Nowack, B., Ranville, J. F., Diamond, S., Gallego-Urrea, J. A., Metcalfe, C., Rose, J., et al. (2012). Potential scenarios for nanomaterial release and subsequent alteration in the environment. *Environ. Toxicol. Chem.* 31, 50–59. doi: 10.1002/etc.726
- Peters, R. J., van Bommel, G., Milani, N. B., den Hertog, G. C., Undas, A. K., van der Lee, M., et al. (2018). Detection of nanoparticles in Dutch surface waters. *Sci. Tot. Environ.* 621, 210–218. doi: 10.1016/j.scitotenv.2017.11.238
- Piccinno, F., Gottschalk, F., Seeger, S., and Nowack, B. (2012). Industrial production quantities and uses of ten engineered nanomaterials in Europe and the world. *J. Nanopart. Res.* 14:1109. doi: 10.1007/s11051-012-1109-9
- Praetorius, A., Scheringer, M., and Hungerbühler, K. (2012). Development of environmental fate models for engineered nanoparticles—A case study of TiO₂ nanoparticles in the Rhine River. *Environ. Sci. Technol.* 46, 6705–6713. doi: 10.1021/es204530n
- Reed, R., Martin, D., Bednar, A., Montañó, M., Westerhoff, P., and Ranville, J. (2017). Multi-day diurnal measurements of Ti-containing nanoparticle and organic sunscreen chemical release during recreational use of a natural surface water. *Environ. Sci. Nano* 4, 69–77. doi: 10.1039/C6EN00283H
- Rubey, W. W. (1933). Settling velocity of gravel, sand, and silt particles. *Am. J. Sci.* 25, 325–338. doi: 10.2475/ajs.s5-25.148.325
- Sani-Kast, N., Scheringer, M., Slomberg, D., Labille, J., Praetorius, A., Ollivier, P., et al. (2015). Addressing the complexity of water chemistry in environmental fate modeling for engineered nanoparticles. *Sci. Tot. Environ.* 535, 150–159. doi: 10.1016/j.scitotenv.2014.12.025
- Scifo, L., Chaurand, P., Bossa, N., Avellan, A., Auffan, M., Masion, A., et al. (2018). Non-linear release dynamics for a CeO₂ nanomaterial embedded in a protective wood stain, due to matrix photo-degradation. *Environ. Pollut.* 241, 182–193. doi: 10.1016/j.envpol.2018.05.045
- Slomberg, D. L., Ollivier, P., Miche, H., Angeletti, B., Bruchet, A., Philibert, M., et al. (2019). Nanoparticle stability in lake water shaped by natural organic matter properties and presence of particulate matter. *Sci. Tot. Environ.* 656, 338–346. doi: 10.1016/j.scitotenv.2018.11.279
- Sun, T. Y., Gottschalk, F., Hungerbühler, K., and Nowack, B. (2014). Comprehensive probabilistic modelling of environmental emissions of engineered nanomaterials. *Environ. Pollut.* 185, 69–76. doi: 10.1016/j.envpol.2013.10.004
- Swanson, H. E., McMurdie, H. F., Morris, M. C., and Evans, E. H. (1969). *Standard X-Ray Diffraction Powder Patterns: Data for 81 Substances*. Washington, DC: National Bureau of Standards. doi: 10.6028/NBS.MONO.25-7
- Thompson, M. E. (1982). “The cation denudation rate as a quantitative index of sensitivity of eastern Canadian rivers to acidic atmospheric precipitation,” in *Long-Range Transport of Airborne Pollutants*, ed H. C. Martin (Dordrecht: Springer), 215–226. doi: 10.1007/978-94-009-7966-6_16
- Vance, M. E., Kuiken, T., Vejerano, E. P., McGinnis, S. P., Hochella, M. F. Jr., Rejeski, D., et al. (2015). Nanotechnology in the real world: Redeveloping the nanomaterial consumer products inventory. *Beilstein J. Nanotechnol.* 6, 1769–1780. doi: 10.3762/bjnano.6.181
- Von der Kammer, F., Ferguson, P. L., Holden, P. A., Masion, A., Rogers, K. R., Klaine, S. J., et al. (2012). Analysis of engineered nanomaterials in complex matrices (environment and biota): general considerations and conceptual case studies. *Environ. Toxicol. Chem.* 31, 32–49. doi: 10.1002/etc.723
- Von der Kammer, F., Legros, S., Hofmann, T., Larsen, E. H., and Loeschner, K. (2011). Separation and characterization of nanoparticles in complex food and environmental samples by field-flow fractionation. *Trends Anal. Chem.* 30, 425–436. doi: 10.1016/j.trac.2010.11.012
- Wang, J., Nabi, M. M., Mohanty, S. K., Nabiul Afrooz, A. R. M., Cantando, E., Aich, N., et al. (2020). Detection and quantification of engineered particles in urban runoff. *Chemosphere* 248, 126070. doi: 10.1016/j.chemosphere.2020.126070
- Westerhoff, P., Song, G., Hristovski, K., and Kiser, M. A. (2011). Occurrence and removal of titanium at full scale wastewater treatment plants: implications for TiO₂ nanomaterials. *J. Environ. Monit.* 13, 1195–1203. doi: 10.1039/c1em10017c

Conflict of Interest: The authors declare that the research was conducted in the absence of any commercial or financial relationships that could be construed as a potential conflict of interest.

Copyright © 2020 Slomberg, Auffan, Guéniche, Angeletti, Campos, Borschneck, Aguerre-Chariol and Rose. This is an open-access article distributed under the terms of the Creative Commons Attribution License (CC BY). The use, distribution or reproduction in other forums is permitted, provided the original author(s) and the copyright owner(s) are credited and that the original publication in this journal is cited, in accordance with accepted academic practice. No use, distribution or reproduction is permitted which does not comply with these terms.